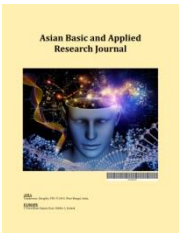

Asian Basic and Applied Research Journal

Volume 6, Issue 1, Page 116-131, 2024; Article no.ABAARJ.1653

Statistical Study of Forbush Effects and Interplanetary Disturbances (FEID) From 1957-2019

V. C. Okoye [a], C. C. Onuchukwu [a*], L. N. Okoli [b] and O. P. Jerry-Okafor [a]

[a] Department of Industrial Physics, Chukwuemeka Odumegwu Ojukwu University, 44221, Awka - Anambra, Nigeria.
[b] Department of Computer Science Education, Madonna University Nigeria, Okija Campus, Anambra State, Nigeria.

Authors' contributions

This work was carried out in collaboration among all authors. All authors read and approved the final manuscript.

Article Information

Open Peer Review History:
This journal follows the Advanced Open Peer Review policy. Identity of the Reviewers, Editor(s) and additional Reviewers, peer review comments, different versions of the manuscript, comments of the editors, etc are available here: https://prh.globalpresshub.com/review-history/1653

Original research Article

Received: 14/06/2024
Accepted: 17/08/2024
Published: 29/08/2024

ABSTRACT

The Forbush effect describes a sudden decrease in cosmic ray intensity on Earth, usually associated with solar storms like coronal mass ejections (CMEs) or solar flares. These events create shock waves that compress the Earth's magnetosphere, reducing cosmic ray influx. Interplanetary disturbances, caused by solar activities, can interact with Earth's magnetosphere, leading to geomagnetic storms associated with the Forbush effect. This study investigates the statistical relationship between the Forbush Effect and various interplanetary disturbance (FIED) parameters from 1957 to 2019. The parameters analyzed include $\mathrm{ABz_{max}}$, $\mathrm{Kp_{max}}$, $\mathrm{KT_{min}}$, $\mathrm{KT_{max}}$, $\mathrm{Be_{max,}}$ $\mathrm{Be_{min}}$, $\mathrm{M_{agn}}$, $\mathrm{A_{xym}}$, $\mathrm{Ap_{max}}$, $\mathrm{Bz_{min}}$, $\mathrm{Az_{range}}$ and SSN. The dataset, which includes 7482

**Corresponding author: Email: onuchukwu71chika@gmail.com;*

Cite as: *Okoye, V. C., C. C. Onuchukwu, L. N. Okoli, and O. P. Jerry-Okafor. 2024. "Statistical Study of Forbush Effects and Interplanetary Disturbances (FEID) From 1957-2019". Asian Basic and Applied Research Journal 6 (1):116-31. https://jofresearch.com/index.php/ABAARJ/article/view/146.*

events, was divided into subsets based on the type of Forbush Decrease (FD): Type 1 (1469) events), Type 2 (34 events), Type 3 (246 events), and Type 9 (5733) events), with a primary focus on Type 1 and Type 9 FD. Between 1957 and the 1980s, Bz values consistently remained around -6 to -7, indicating a predominantly southward orientation; however, post-1986, these values became more variable, with a range from -3.8 to -6.7 observed between 2010 and 2019. The $\mathrm{ABz_{max}}$ values varied from 2.6 nT to 9.6 nT during the late 1960s to the early 1980s, shifted to a range of 6.0 nT to 9.8 nT between 1986 and 2010, and after 2010, they ranged from 4.9 nT to 6.8 nT, including an unusual negative value of -4.8 nT in 2010. Peaks in $\mathrm{Be_{max}}$ were particularly noticeable during the years 1971, 1972, 1975, 1976, the late 1980s, and 1995-1997, with an outlier occurring in 2009. Mean $\mathrm{KT_{max}}$ values fluctuated significantly, with peaks observed in 1966, followed by a minimum in 2014, while mean $\mathrm{KT_{min}}$ values showed low variability until a significant spike in 1986, followed by a sharp decline in 2014, after which they remained consistently low. $\mathrm{Ap_{max}}$ mean values, which peaked in the late 1950s and early 1960s, reached a high of 68.3 in 1960 before declining to 18.0 in 1965; subsequent fluctuations continued through the 1970s and 1980s, with a low of 4.0 in 1986, and post-1986 values varied between 15-50, generally decreasing to 18.1 by 2019. $\mathrm{KP_{max}}$ values typically ranged from 4.0 to 5.0, with significant spikes in 1986 (44.6) and 2010 (55.3), indicating intense geomagnetic events. $\mathrm{A_{xym}}$ values remained relatively stable between 1.0 and 1.6, except for significant spikes in 1986 (59.4) and 2010 (21.4). $\mathrm{M_{agn}}$ mean values ranged between 1.2 to 1.5, with periodic spikes and dips. In general, Type 1 events exhibited considerable variability with irregular fluctuations, lacking a clear trend, while Type 9 events displayed more stable behavior with minor fluctuations, demonstrating a consistent and predictable pattern. Across all parameters, consistent trends were observed, with Type 1 and Type 9 events differing primarily in the strength of the correlations. Our analytical approach included descriptive statistics such as distribution plots, central tendency estimations (mean and median), and time series plots to identify annual patterns. Additionally, correlation analyses were conducted to elucidate relationships among the parameters. This extended analysis aims to provide deeper insights into the mechanisms linking interplanetary disturbances with cosmic ray modulation, offering implications for space weather prediction and our understanding of solar-terrestrial interactions.

Keywords: Forbush decrease; interplanetary disturbance; data analysis; geomagnetic index.

1. INTRODUCTION

The Forbush Effect is a temporary reduction in cosmic ray flux observed on Earth following a solar coronal mass ejection (CME). This reduction, known as Forbush Decrease (FDs), results from the solar wind and magnetic field interactions that modulate the galactic cosmic ray intensity within our planet's magnetosphere. This paper aims to dissect the temporal and spatial characteristics of Forbush Effects and unravel the underlying mechanisms that govern their manifestation. The investigation into Forbush Effects and Interplanetary Disturbances (FIED) spanning 1957-2019 is a meticulous exploration of celestial phenomena with profound implications for space weather science. Forbush noted a reciprocal relationship between Earth's cosmic ray intensity and the 11-year solar cycle of sunspot activity. Since their initial discovery, thousands of such events have been meticulously observed [1-11].

Interplanetary disturbances, arising from disturbances in the solar wind and interplanetary magnetic field, can emanate from various solar events, such as solar flares, coronal holes, and CMEs. Understanding these distinctions is vital for predicting and interpreting the impact of interplanetary disturbances on Forbush Effects. The study leverages a comprehensive dataset compiled from the Forbush Effects and Interplanetary Disturbance database, spanning over six decades, to conduct a detailed statistical analysis of the temporal trends, frequency, and magnitude of Forbush Effects and associated interplanetary disturbances [12-16].

Various researchers [17-28] have worked on multiple aspects of FDs and interplanetary disturbances in various solar cycles e.g. [17,23], worked on the relationship between different parameters (magnetic flux of solar eruptions and the Ap index of geomagnetic storms e.g. [18]), cosmic ray variations and magnetic clouds [19,20], research on different types of Forbush effect and solar phenomena e.g. [21-22,24], Dependence of Forbush-decrease characteristics on parameters of solar eruptions e.g. [25], study

FDs and geomagnetic storms and related phenomena [26-28].

Our present investigation leverages a comprehensive dataset compiled from the Forbush Effects and Interplanetary Disturbance database, spanning over six decades. This rich repository contains a wealth of information, enabling us to conduct a detailed statistical analysis of the temporal trends, frequency, and magnitude of Forbush Effects and associated interplanetary disturbances [10,13,14]. The global survey method, utilizing data from approximately 40 neutron monitors, enhances the precision of estimating cosmic ray (CR) density variations and facilitates the differentiation between isotropic and anisotropic components [3,15,16].

We further classify Forbush Effects based on their onset characteristics, distinguishing between sudden storm commencements (SSCs) and gradual commencements (GCs). This classification provides valuable insights into the dynamic nature of Forbush Effects, shedding light on the diverse mechanisms triggering these cosmic phenomena [29].

2. MATERIALS AND METHODS

2.1 Materials

The dataset utilized in this research was acquired from the Forbush Effects and Interplanetary Disturbances database, accessible at http://spaceweather.izmiran.ru/eng/dbs.html, established and meticulously maintained by IZMIRAN (http://spaceweather.izmiran.ru/eng/dbs.html) [13,14,10]. This comprehensive database incorporates FD parameters derived from the global neutron monitor network's data, employing the global survey method for particles with rigidity of 10 GV [3,16,30]. The global survey method, utilizing data from approximately 40 neutron monitors, enhances the precision of estimating cosmic ray (CR) density variations and facilitates the differentiation between isotropic and anisotropic components. Additionally, the Forbush Effects and Interplanetary Disturbances database encompasses geomagnetic indices, solar wind parameters, and solar geophysical data. Sunspot numbers were also obtained from SILSO data/image, Royal Observatory of Belgium, Brussels, accessible at https://www.sidc.be/silso/extheminum [31].

- ABz_{max}: the maximal absolute value of the Bz component of the IMF.
- KT_{max} : the maximum value of the ratio (KT) of the observed hourly average temperature of the solar wind to the temperature, calculated from the velocity of the solar wind (SW).
- KT_{min}: minimal value of the ratio (KT) of the observed hourly average temperature of the solar wind to the temperature, calculated from the velocity of the solar wind (SW).
- Be_{max}: maximal hourly plasma Beta in the event.
- Be_{Min}: minimal hourly plasma Beta in the event.
- M_{agn}: FD magnitude for particles with 10 GV rigidity, calculated as maximal range CR density variations in the event, obtained by GSM from NM network data.
- Kp_{max}: maximal Kp-index in the event
- A_{xym} : maximal value of the equatorial component of the CR vector anisotropy in the event (in %)
- Ap_{max} : maximal 3-hour Ap-index in the event.
- Bz_{min}: minimal hourly Bz component of the IMF in the event.
- Az_{range} : Range of the north-south component variation of the CR vector anisotropy in the event (in %).
- SSN: The number of sunspots at the FD onset day

There are 2 main classifications of FD events based on the type of onset (OTypes) and the solar sources (STypes). Our analysis will be based on the onset classification given in Table 1, based on the total number of events for different types we will concentrate on all events (7482), Type 1 (3469), and Type 9 (5733) events.

2.2 Methods

We analyze the data by plotting the time series graph and performing simple linear correlation analysis to check for possible correlation between the parameters. Time series analysis is a specific way of analyzing a sequence of data points collected over an interval of time. In time series analysis, analysts record data points at consistent intervals over a set period rather than just recording the data points intermittently or randomly. Time series analysis typically requires a large number of data points to ensure consistency and reliability. An extensive data set ensures you have a representative sample size and that analysis can cut through noisy data.

Table 1. FD classification based on the onset type

OType	Number	Description
Type 1	1469	FD onset with Interplanetary Shock Waves (ISW) and Storm Sudden Commencement (SSC)
Type 2	34	FD onset with Interplanetary Shock Wave (ISW)
Type 3	246	FD onset with weak Storm Sudden Commencement (SSC)
Type 9	5733	FD onset without interplanetary shock wave (ISW) and storm sudden commencement (SSC)

Correlation quantifies the extent of the linear relationship between two or more variables, indicating how changes in one variable are related to changes in another, either in the same or opposite direction. The correlation coefficient, denoted as r, represents the strength of this linear relationship between two variables, X and Y. The degree of this correlation is measured using the Pearson product-moment correlation coefficient, which is given as [e.g. 32]

$$r = \frac{\sum_{i=1}^{n}(X_i-\bar{X})(Y_i-\bar{Y})}{\sqrt{\sum_{i=1}^{n}(X_i-\bar{X})^2(Y_i-\bar{Y})^2}} \quad (1)$$

where n is the number of each variable which must be equal, $\bar{X}$ and $\bar{Y}$ are the mean value of the variable X and Y respectively. Interpretation of r: $r = +1$, which implies that there is a perfect positive (direct) relationship ; $r = -1$, which implies a perfect negative (indirect) relationship; $-1.0 < r < -0.5$, implies there is a strong negative linear relationship; $-0.5 \leq r \leq -0.3$, implies there is a weak negative relationship; $+0.3 \leq r \leq +0.5$; implies there is a weak positive linear relationship $+0.5 \leq r \leq 1$, implies there is a strong positive linear relationship; $r < \pm 0.3$ implies there is no relationship between the two variables.

3. RESULTS AND DISCUSSION

3.1 Results

In Fig. 1(a), the time series graph of mean and median values of the minimal hourly Bz component of the IMF from 1957 to 2019 shows significant fluctuations. From 1957 to the mid-1980s, Bz values were mostly around -6 to -7, indicating a southward orientation. After 1986, the values became more variable, with a mix of highly negative and occasional positive values. In recent years (2010-2019), values have been moderately negative. Overall, the data highlights the variability in IMF orientation, which influences geomagnetic disturbances and storms. After the early 2000s, Bz values stabilized within a range of -3.8 to -6.7, indicating a relatively stable, predominantly negative trend.

Fig. 1(b) presents the time series graph of the mean and median values of the maximal absolute Bz component of the IMF $A\mathrm{Bz}_{\max}$ from 1957 to 2019. The analysis shows considerable variability, with a lower range of 2.6 nT to 9.6 nT from the late 1960s to early 1980s, occasional peaks in the late 1970s and early 1980s, and stabilization within 6.0 nT to 9.8 nT from 1986 to 2010. Post-2010, there's a notable decrease, with values ranging from 4.9 nT to 6.8 nT, including a negative -4.8 nT in 2010. The median values also show variability, with consistent ranges from the mid-1960s to mid-1970s, peaks in the late 1970s, and a general decline post-1995, particularly after 2010, indicating a potential weakening of the IMF Bz component.

Fig. 1(c) shows the time series graph of mean and median values for the minimal value of maximal hourly plasma Beta ($\mathrm{Be}_{\max}$) from 1957 to 2019. The data exhibits intermittent spikes and fluctuations, with notable peaks in 1971, 1972, 1975, 1976, the late 1980s, 1995-1997, and an outlier in 2009. There is no consistent trend, as the values show irregular variations over the years, characterized by sporadic peaks and falls. The median values also reflect this irregularity, with significant spikes and periods of higher or lower values, but no clear continuous trend.

Fig. 1(d) illustrates the mean and median values for the minimal value of minimal hourly plasma Beta ($\mathrm{Be}_{\mathrm{Min}}$) from 1957 to 2019, showing variable trends with occasional fluctuations and intermittent peaks. Significant anomalies are observed in 1969 and 2010, with values of 18.6 and 10.8, respectively. The data indicates periods of stability, particularly in the early 1960s, and sporadic increases and decreases in subsequent decades. Notable low and high values are seen in 1986, 1995, and 1996. From the early 2000s onward, there is a tendency toward lower values with occasional peaks. Overall, the trend appears irregular, lacking a

consistent pattern, and showing sporadic fluctuations throughout the period. Median values also exhibit an erratic yet discernible trend with occasional spikes and relative stability interspersed with deviations, notably in 2010.

Fig. 2 (a) is the time series graph that shows mean and median values for the maximal ratio (KT) of observed hourly average temperature to solar wind temperature from 1957 to 2019. Mean KT_{max} values exhibit notable fluctuations, with peaks in 1966 and a minimum in 2014. Median KT_{max} values also show variability, with periods of stability and spikes, particularly in the 1960s and 1970s.

Fig. 2 (b) is the time series graph that shows the mean and median values for the minimal ratio (KT) of observed hourly average temperature to solar wind temperature from 1957 to 2019. Mean KT_{min} values have low variability until a significant spike in 1986 and a sharp drop in 2014, remaining low afterward. Median KT_{min} values follow a similar pattern, with substantial fluctuations and notable anomalies in 1986 and 2014.

Fig. 2(c) presents the time series graph of mean and median values of the maximal 3-hour Ap-index (Ap_{max},) from 1957 to 2019. The mean values peaked in the late 1950s and early 1960s, reaching 68.3 in 1960, then declined to 18.0 in 1965. Fluctuations continued through the 1970s and 1980s, with a significant low of 4.0 in 1986. Post-1986, the values varied between 15 to 50 until the early 2000s, then generally decreased, ending at 18.1 in 2019. The median values follow a similar pattern, peaking around 48.0 in the early 1960s, dropping significantly in 1965 and 1986, peaking again in 1983 and 2003, then declining towards the 2010s. Overall, the Ap_{max} values show notable variations with intermittent peaks and drops, reflecting shifts in geomagnetic activity over the years.

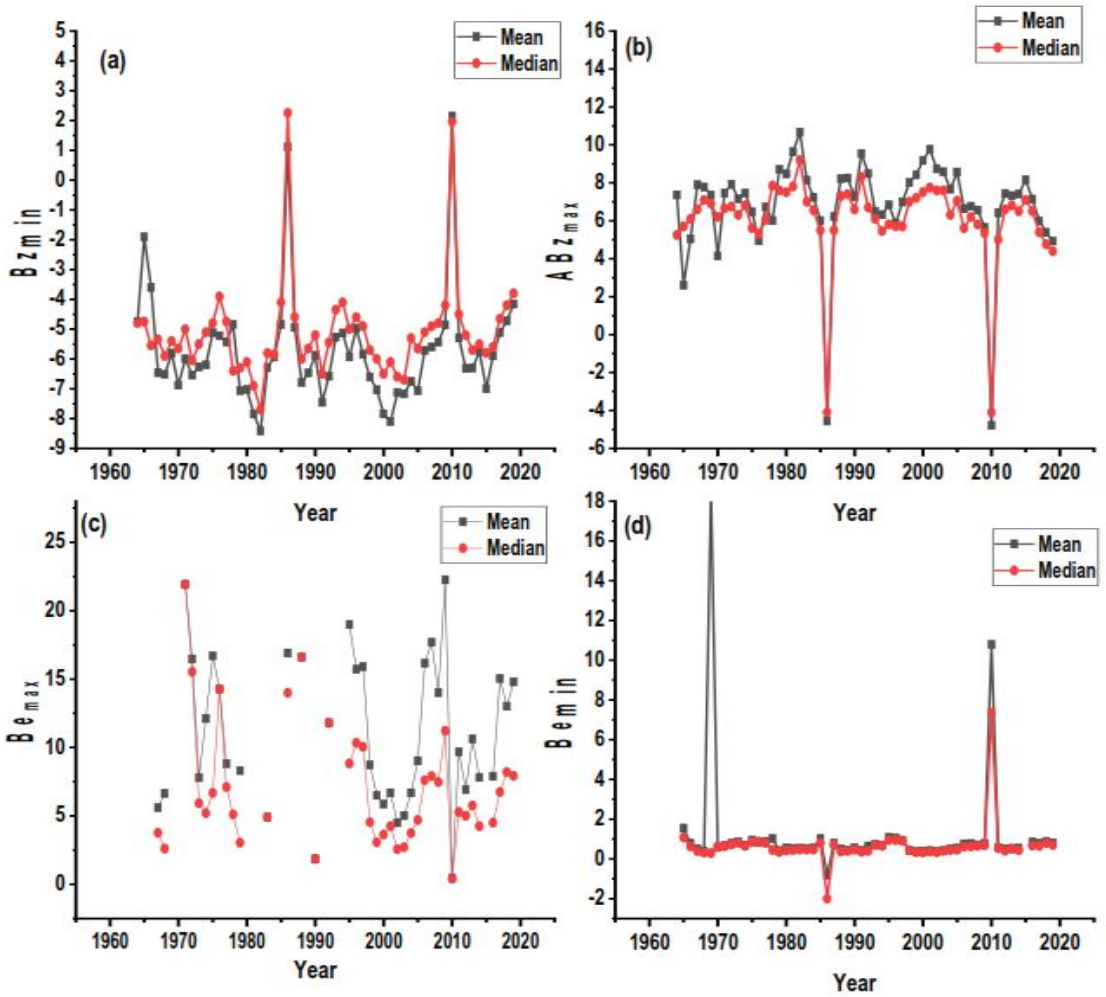

Fig. 1. Time series graph of mean and median of $\mathbf{Bz_{min}}$, $\mathbf{ABz_{max}}$, $\mathbf{Be_{max}}$, $\mathbf{Be_{Min}}$

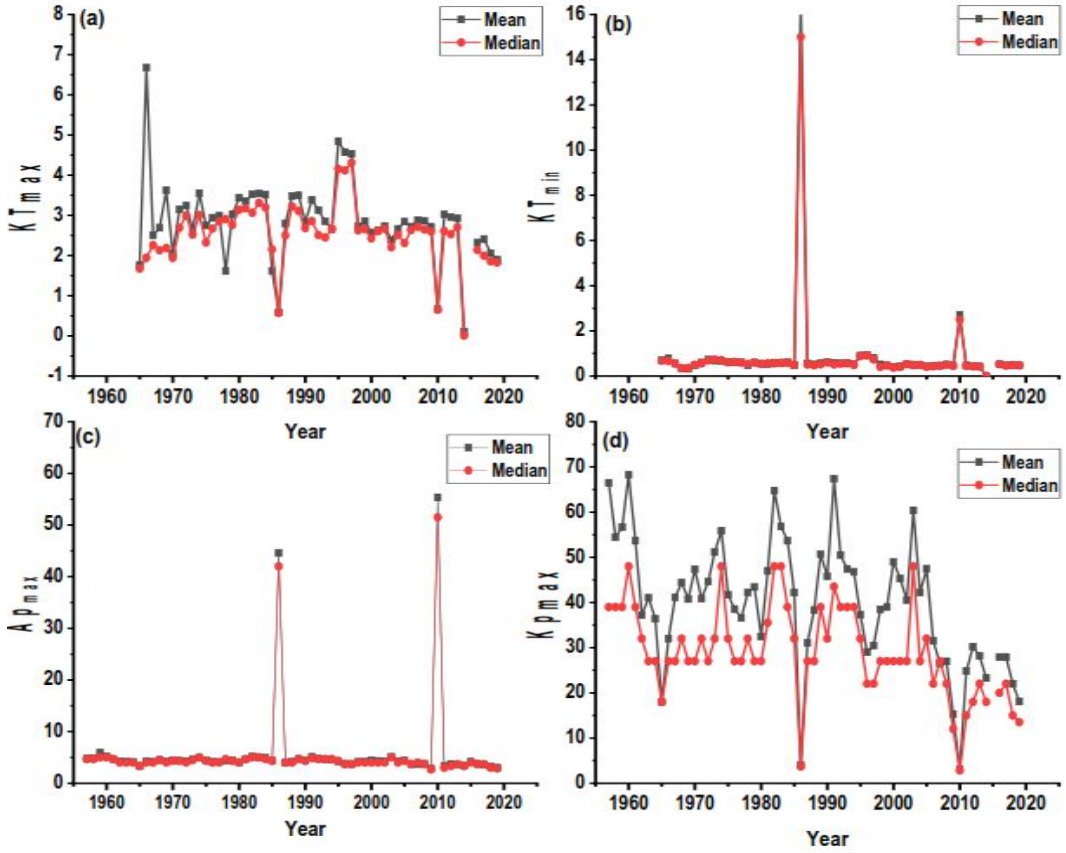

Fig. 2. The time series graph of the mean and median of KT_{max}, KT_{min}, Ap_{max}, and Kp_{max} from 1957 -2019

Fig. 2(d) shows the mean and median values of the maximal Kp-index from 1957 to 2019, indicating fluctuations and notable trends. Most years exhibit moderate geomagnetic disturbances with Kp_{max} values around 4.0 to 5.0. Significant spikes occurred in 1986 (44.6) and 2010 (55.3), indicating intense geomagnetic events. Median values also show general stability around 3.7 to 4.7, with peaks in 1986 (42.0) and 2010 (51.5). Overall, the data highlights periods of stability with occasional significant geomagnetic disturbances.

In Fig. 3(a), the time series graph illustrates the mean and median values of the maximal equatorial component of the cosmic ray (CR) vector anisotropy (A_{xym},) from 1957 to 2019. Generally, values remain stable between 1.0 and 1.6, but significant spikes occur in 1986 (59.4) and 2010 (21.4). Median values show similar trends, with major anomalies in 1986 (62.0) and 2010 (20.5). Recent years exhibit occasional higher values and minor fluctuations, maintaining overall stability with intermittent spikes and decreases.

Fig. 3(b) is the time series graph of mean and median values of Forbush decrease magnitude for particles with 10 GV rigidity (M_{agn}) from 1957 to 2019 illustrates fluctuating patterns. Mean values range around 1.2 to 1.5, with periodic spikes and dips. There was a gradual decline from the late 1950s to the mid-1960s, followed by increases and fluctuations until the late 1980s. The years post-2000 show moderate variations, with a decreasing trend towards 2019 (0.6), indicating substantial fluctuations in cosmic ray density variations over time.

Fig. 3(c) is the time series graph of mean and median values of the north-south component variation of the CR vector anisotropy (Az_{range})) from 1957 to 2019 shows fluctuating patterns. Mean values ranged from 0.6% to 3.2%, with higher values in the late 1950s, declining until the mid-1960s. After fluctuating between 1.0% and 1.6% from the late 1960s to the early 1980s, a declining trend continued until 2019. Median values also exhibited variability, initially higher and then stabilizing around 1.4%, with a notable drop to 0.7% in 1986 and a general decrease afterward.

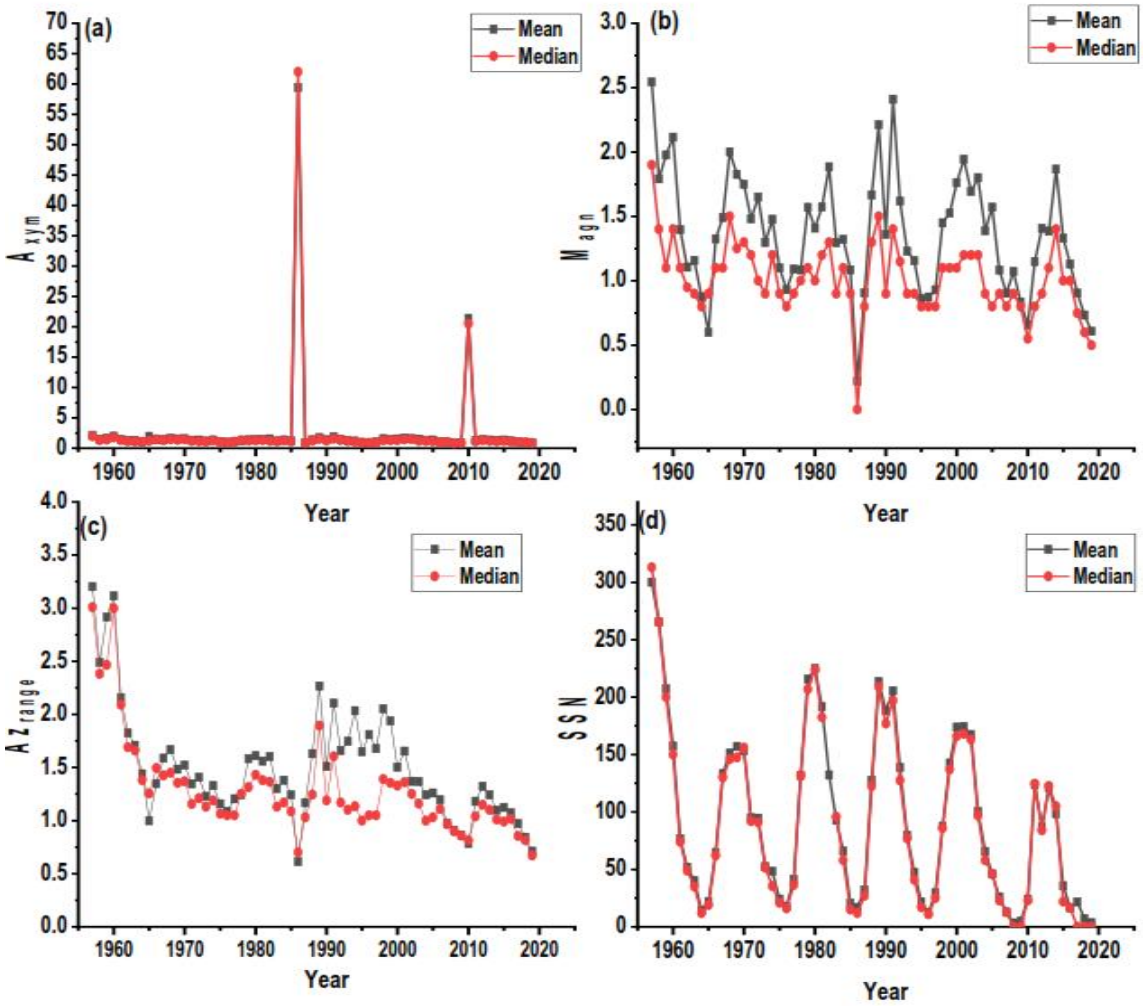

Fig. 3. Time series graph of mean and median of A_{xym}, M_{agn}, Az_{range} and SSN from 1957 -2019

Fig. 3(d) is the time series graph of mean and median values of the number of sunspots at Forbush decrease onset days (SSN) from 1957 to 2019 showing notable fluctuations and a downward trend. Initially high SSN values (150-300) in the late 1950s and early 1960s decreased to as low as 3.3-12.3 by the mid-1980s. A slight recovery occurred in the mid-1990s to early 2000s, but values remained low (3.6-174.4). Median SSN values also declined significantly, with high values in the late 1950s dropping to zero counts by the mid-2000s, indicating a prolonged period of low solar activity.

In Fig. 4 (a), the mean values of the minimal hourly Bz component of the IMF for Type 1 and Type 9 Forbush events from 1957 to 2019 reveal distinct patterns. Type 1 events show dynamic fluctuations, with values ranging from highly negative to occasionally positive, particularly from the late 1950s to the mid-1980s and again from the mid-1990s onwards. In contrast, Type 9 events exhibit a more consistent trend, predominantly maintaining moderately negative values throughout the period, with minimal extreme deviations. Overall, Type 1 events demonstrate greater variability, while Type 9 events display a stable, moderately negative trend.

In Fig. 4 (b) the mean values of the maximal absolute value of the Bz component of the Interplanetary Magnetic Field (IMF), specifically for Type 1 and Type 9 Forbush events, display distinct patterns. Type 1 events exhibit considerable variability with irregular fluctuations, while Type 9 events show a more stable behavior with minor fluctuations. Overall, type 1 Forbush events manifest higher variability, lacking a coherent trend, whereas type 9 events

demonstrate a more stabilized pattern with fewer extreme values.

In Fig. 4 (c), there are noticeable fluctuations with periodic peaks for Type 1 Forbush events, while Type 9 events showcase a more varied pattern with sporadic high values. Type 9 events consistently manifest higher plasma Beta values compared to Type 1 events throughout various periods, indicating distinct characteristics and likely different underlying causal factors between these two types of Forbush events.

In Fig. 4 (d), the mean values of minimal hourly plasma Beta in the event (Be_{min}) from 1957 to 2019, were plotted for Type I and Type 9 Forbush events exhibit fluctuations. Type 1 events display a relatively stable pattern, while Type 9 events show greater variability and extreme fluctuations, notably in 1986. Both types show an increasing trend in mean values, with Type 1 events demonstrating a more gradual increase.

Fig. 5(a) presents the mean values of the maximum ratio (KT_{max}) of observed hourly average temperatures from 1957 to 2019 for Type 1 and Type 9 Forbush events. Type 1 events show erratic fluctuations, ranging widely and lacking a clear trend, indicating unpredictable temperature impacts. In contrast, Type 9 events maintain a stable range of (KT_{max})values, typically between 1 and 4.5, demonstrating a consistent and predictable influence on temperature patterns. Despite overall stability, both event types occasionally exhibit extreme high or low (KT_{max}) values due to potential external factors.

Fig. 5(b) depicts the mean values of the minimum ratio (KT_{min}) of observed hourly average temperatures from 1957 to 2019 for Type 1 and Type 9 Forbush events. Type 1 events display a wide range of KT_{min}, values with notable fluctuations, from extremely low (0.00214 in 2014) to moderate (0.7356 in 1965), showing an inconsistent pattern without a clear trend. Conversely, Type 9 events show more stability, generally hovering around moderate values with fewer extreme fluctuations. Overall, Type 1 events exhibit greater variability and erratic fluctuations compared to the more stable and consistent patterns seen in Type 9 events.

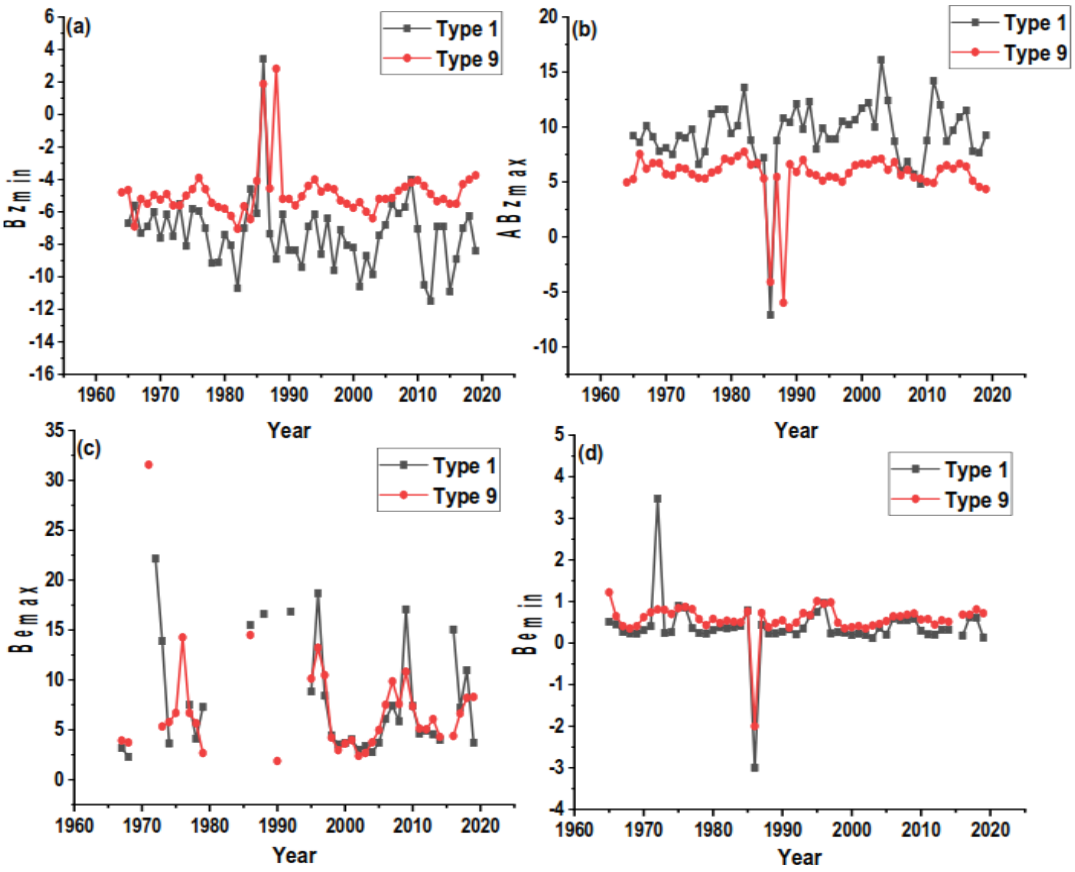

Fig. 4(a-d). The Time series graph of the mean Bz_{min}, ABz_{max}, Be_{max}, and Be_{min}, for Types 1 and 9 events

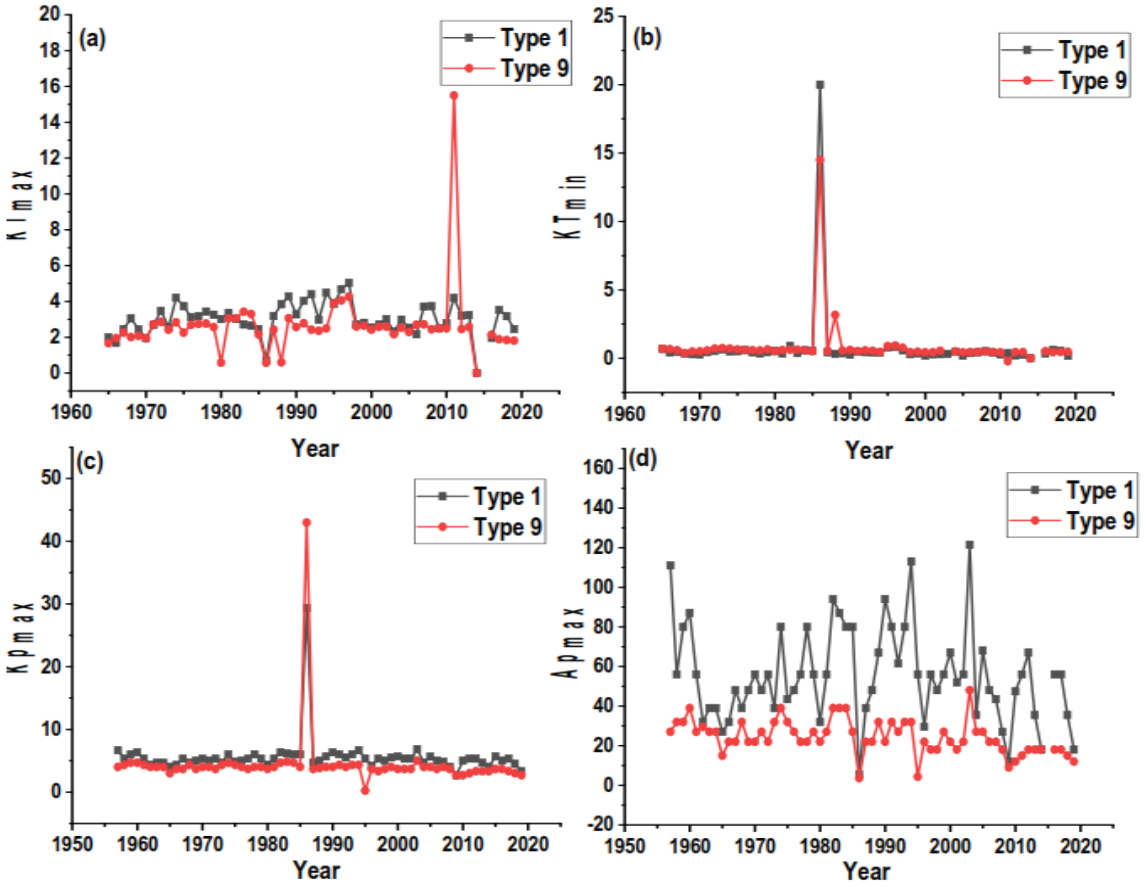

Fig. 5. Shows the time series graph of the mean of KT_{max}, KT_{min}, Ap_{max}, and Kp_{max} for Types 1 and 9 events from 1957 -2019

In Fig. 5 (c) Maximal 3-hour Ap-index, Type 1 Forbush events show greater variability and higher mean maximal 3-hour Ap-index values compared to Type 9 events, indicating a stronger impact on geomagnetic activity. Type 1 events exhibit wider swings and notable spikes, while Type 9 events maintain a more stable pattern with fewer extreme fluctuations. Both types have periods of increase and decrease, with Type 1 events showing a slight decreasing trend and Type 9 events remaining stable.

In Fig. 5 (d) the Maximal Kp-index, Type 1 Forbush events generally exhibit higher and more variable mean maximal Kp-index values compared to Type 9 events. Type 1 events range broadly, peaking at 28.1375 in 1986, while Type 9 events have a narrower range, peaking at 4.78911 in 1984. Both event types show a decrease in the early 1990s, a rise in the mid-1990s, and stability from 2000 onwards.

In Fig. 6 (a) Maximal Value of Equatorial Component of CR Vector Anisotropy Type 1 Forbush events show mean values ranging from 0.9% to 2.5%, with sporadic peaks and a general decline towards lower percentages around 1% or slightly below from 2016 to 2019. In contrast, Type 9 Forbush events range from 0.8% to 1.8%, exhibiting fewer extreme fluctuations and a relatively stable trend across the years. While Type 1 events display more significant variations and occasional peaks, Type 9 events maintain a consistent average with a smoother trajectory. Overall, Type 1 events are more erratic, whereas Type 9 events show stable values.

Fig. 6(b), shows the mean values of Forbush decrease magnitude for particles with 10 GV rigidity, calculated as maximal range CR density variations in the event (M_{agn}), from 1957 to 2019 for Type I and Type 9 Forbush events, reveal differences. Type 1 events consistently exhibit higher mean values compared to Type 9 events, indicating larger maximal range cosmic ray density variations. Type 1 events showcase significant fluctuations, whereas Type 9 events maintain a more consistent and steadier trend over the observed period, with lower mean values consistently in the 2010s.

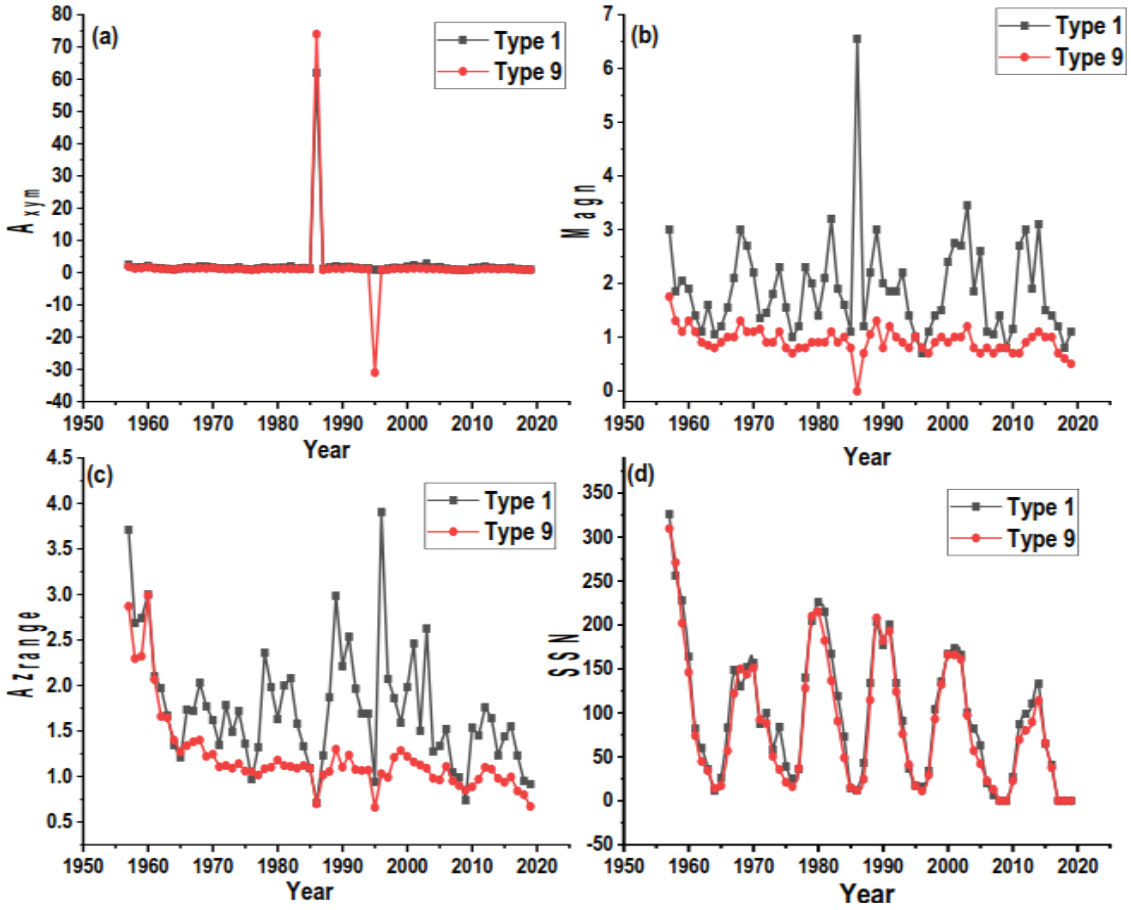

Fig. 6. The time series graph of the mean of A_{xym}, M_{agn}, Az_{range} and SSN for Type 1 and Type 9 events from 1957 -2019

In Fig. 6(c), we show the range of North-South Component Variation of CR Vector Anisotropy, Type 1 Forbush events generally show higher and more erratic values in the range of the north-south component variation of CR vector anisotropy compared to Type 9 events. Both types exhibit fluctuations over the years, with Type 9 events showing a steadier decline from the late 1950s to the late 1970s and a stable trend afterward. Both types display an overall decreasing trend from their peaks, with Type 1 events fluctuating more prominently than Type 9 events. From the mid-1970s onward, Type 9 events consistently displayed lower values compared to Type 1 events.

Fig. 6 (d) Range of Number of Sunspots at Forbush Decrease Onset Day (SSN), Type 1 Forbush events exhibit higher mean SSN values compared to Type 9 events across the years. Both types display higher SSN values in the late 1950s and early 1960s, with a notable decrease in the mid-1960s, followed by an increase until the late 1970s. Afterward, Type 1 events maintain relatively higher and more fluctuating SSN values, while Type 9 events show a consistent decline until the early 2000s. Both types show lower and fluctuating SSN values post-2000, with no recorded SSN values since 2017. Overall, Type 1 events consistently demonstrate higher SSN values, while Type 9 events exhibit lower and gradually decreasing SSN values, especially from the late 1970s to the early 2000s.

In Tables 2-4, we displayed the Pearson correlation coefficients calculated using the yearly mean values of 12 FEID parameters: Bz_{min}, ABz_{max}, KT_{max}, KT_{min} Be_{max}, Be_{Min}, , M_{agn}, Kp_{max}, Ap_{max}, A_{xym} , Az_{range}, SSN records spanning 1957 to 2019 for all the events, Type 1 and Type 9 events respectively.

Table 2. Pearson Correlations coefficients of yearly mean FEID parameters (1957-2019)

	1	2	3	4	5	6	7	8	9	10	11	12
1	1.0	-1.0	-0.4	0.6	0.1	0.3	-0.7	0.8	-0.7	0.7	-0.6	-0.5
2	-1.0	1.0	0.4	-0.7	-0.1	-0.3	0.7	-0.8	0.7	-0.7	0.6	0.5
3	-0.4	0.4	1.0	-0.3	0.3	0.0	0.2	-0.4	0.3	-0.4	0.4	0.1
4	0.6	-0.7	-0.3	1.0	0.2	0.0	-0.4	0.7	-0.4	1.0	-0.3	-0.2
5	0.1	-0.1	0.3	0.2	1.0	-0.3	-0.5	-0.2	-0.3	0.0	-0.2	-0.5
6	0.3	-0.3	0.0	0.0	-0.3	1.0	0.0	0.3	-0.2	0.1	-0.1	0.1
7	-0.7	0.7	0.2	-0.4	-0.5	0.0	1.0	-0.3	0.8	-0.3	0.7	0.8
8	0.8	-0.8	-0.4	0.7	-0.2	0.3	-0.3	1.0	-0.4	0.8	-0.2	-0.1
9	-0.7	0.7	0.3	-0.4	-0.3	-0.2	0.8	-0.4	1.0	-0.4	0.7	0.6
10	0.7	-0.7	-0.4	1.0	0.0	0.1	-0.3	0.8	-0.4	1.0	-0.2	-0.1
11	-0.6	0.6	0.4	-0.3	-0.2	-0.1	0.7	-0.2	0.7	-0.2	1.0	0.7
12	-0.5	0.5	0.1	-0.2	-0.5	0.0	0.8	-0.1	0.6	-0.1	0.7	1.0

The columns/rows represent $1 = Bz_{min}; 2 = ABz_{max}; 3 = KT_{max}; 4 = KT_{min}; 5 = Be_{max}; 6 = Be_{min}; 7 = M_{agn}; 8 = Kp_{max}; 9 = Ap_{max}; 10 = A_{xym}; 11 = Az_{range}; 12 = SSN$

Table 3. Pearson Correlations coefficients of yearly mean FEID parameters for Type 1 events (1957-2019)

	1	2	3	4	5	6	7	8	9	10	11	12
1	1.0	-0.9	-0.3	0.6	0.5	-0.5	-0.2	0.5	-0.6	0.6	-0.4	-0.4
2	-0.9	1.0	0.3	-0.7	-0.4	0.6	0.2	-0.6	0.6	-0.7	0.5	0.4
3	-0.3	0.3	1.0	-0.3	0.1	0.4	-0.3	-0.3	0.2	-0.3	0.3	-0.1
4	0.6	-0.7	-0.3	1.0	0.2	-1.0	0.3	1.0	-0.3	1.0	-0.3	-0.2
5	0.5	-0.4	0.1	0.2	1.0	-0.1	-0.3	0.1	-0.3	0.2	-0.1	-0.4
6	-0.5	0.6	0.4	-1.0	-0.1	1.0	-0.5	-1.0	0.3	-1.0	0.2	0.1
7	-0.2	0.2	-0.3	0.3	-0.3	-0.5	1.0	0.5	0.5	0.4	0.4	0.6
8	0.5	-0.6	-0.3	1.0	0.1	-1.0	0.5	1.0	0.1	1.0	0.1	0.1
9	-0.6	0.6	0.2	-0.3	-0.3	0.3	0.5	0.1	1.0	-0.2	0.6	0.5
10	0.6	-0.7	-0.3	1.0	0.2	-1.0	0.4	1.0	-0.2	1.0	-0.2	-0.1
11	-0.4	0.5	0.3	-0.3	-0.1	0.2	0.4	0.1	0.6	-0.2	1.0	0.7
12	-0.4	0.4	-0.1	-0.2	-0.4	0.1	0.6	0.1	0.5	-0.1	0.7	1.0

The columns/rows represent $1 = Bz_{min}; 2 = ABz_{max}; 3 = KT_{max}; 4 = KT_{min}; 5 = Be_{max}; 6 = Be_{min}; 7 = M_{agn}; 8 = Kp_{max}; 9 = Ap_{max}; 10 = A_{xym}; 11 = Az_{range}; 12 = SSN$

Table 4. Pearson Correlations coefficients of yearly mean FEID parameters for Type 9 events (1957-2019)

	1	2	3	4	5	6	7	8	9	10	11	12
1	1.0	-1.0	-0.4	0.8	0.3	-0.3	-0.7	0.8	-0.6	0.8	-0.4	-0.5
2	-1.0	1.0	0.4	-0.9	-0.3	0.4	0.7	-0.8	0.6	-0.9	0.4	0.5
3	-0.4	0.4	1.0	-0.3	0.2	0.3	0.2	-0.4	0.4	-0.4	0.5	0.2
4	0.8	-0.9	-0.3	1.0	0.1	-0.6	-0.5	1.0	-0.4	1.0	-0.3	-0.2
5	0.3	-0.3	0.2	0.1	1.0	0.3	-0.4	0.1	-0.2	0.1	-0.2	-0.6
6	-0.3	0.4	0.3	-0.6	0.3	1.0	0.0	-0.7	0.1	-0.7	0.1	-0.4
7	-0.7	0.7	0.2	-0.5	-0.4	0.1	1.0	-0.4	0.6	-0.4	0.6	0.7
8	0.8	-0.8	-0.4	1.0	0.1	-0.7	-0.4	1.0	-0.3	1.0	-0.2	-0.1
9	-0.6	0.6	0.4	-0.4	-0.2	0.1	0.6	-0.3	1.0	-0.4	0.5	0.3
10	0.8	-0.9	-0.4	1.0	0.1	-0.7	-0.4	1.0	-0.4	1.0	-0.2	-0.1
11	-0.4	0.4	0.5	-0.3	-0.2	0.1	0.6	-0.2	0.5	-0.2	1.0	0.6
12	-0.5	0.5	0.2	-0.2	-0.6	-0.4	0.7	-0.1	0.3	-0.1	0.6	1.0

The columns/rows represent $1 = Bz_{min}; 2 = ABz_{max}; 3 = KT_{max}; 4 = KT_{min}; 5 = Be_{max}; 6 = Be_{min}; 7 = M_{agn}; 8 = Kp_{max}; 9 = Ap_{max}; 10 = A_{xym}; 11 = Az_{range}; 12 = SSN$

3.2 Discussion

From the correlation coefficient results displayed in Table 2,

- Bz_{min} showed a strong negative correlation with ABz_{max} , a positive correlation with KT_{min} (r = 0.6), Kp_{max} (r = 0.8), and A_{xym} (r = 0.7), a negative correlation with M_{agn} (r = -0.7), Ap_{max} (r = -0.7), and Az_{range} (r = -0.6) and a moderate negative correlation with SSN (r = -0.5).
- ABz_{max} showed a strong negative correlation with Bz_{min} , a positive correlation with KT_{max} (r = 0.4), M_{agn} (r = 0.7), Ap_{max} (r = 0.7), Az_{range} (r = 0.6), and SSN (r = 0.5) and also a negative correlation with KT_{min} (r = -0.7), Kp_{max} (r = -0.8), and A_{xym} (r = -0.7).
- KT_{max} shows a positive correlation with ABz_{max} (r = 0.4), Ap_{max} (r = 0.3), and Az_{range} (r = 0.4), a negative correlation with B_{zmin} (r = -0.4 Kp_{max} (r = -0.4), and A_{xym} (r = -0.4).
- KT_{min} showed a positive correlation with Bz_{min} (r = 0.6), Kp_{max} (r = 0.7), and A_{xym} (r = 1.0), a negative correlation with ABz_{max} (r = -0.7), M_{agn} (r = -0.4), Ap_{max} (r = -0.4), and Az_{range} (r = -0.3).
- Be_{max} showed a weak correlation with most parameters, a negative correlation with M_{agn} (r = -0.5), Ap_{max} (r = -0.3), and SSN (r = -0.5)
- B_{zmin} showed very weak correlations with most parameters, except with Bz_{min} (r = 0.3) and Kp_{max} (r = 0.3) which were positive correlations.
- M_{agn} positive correlation with ABz_{max} (r = 0.7), Ap_{max} (r = 0.8), Az_{range} (r = 0.7), and SSN (r = 0.8), a negative correlation with Bz_{min} (r = -0.7), KT_{min} (r = -0.4), and Kp_{max} (r = -0.3).
- Kp_{max} showed a positive correlation with B_{zmin} (r = 0.8), KT_{min} (r = 0.7), A_{xym} (r = 0.8), a negative correlation with ABz_{max} (r = -0.8), KT_{max} (r = -0.4), and M_{agn} (r = -0.3).
- Ap_{max}, displayed a positive correlation with ABz_{max} (r = 0.7), M_{agn} (r = 0.8), Az_{range} (r = 0.7), and SSN (r = 0.6), but a negative correlation with Bz_{min} (r = -0.7), KT_{min} (r = -0.4), and K_{pmax} (r = -0.4).
- A_{xym} showed a positive correlation with Bz_{min} (r = 0.7), KT_{min} (r = 1.0), Kp_{max} (r = 0.8), and a negative correlation with ABz_{max} (r = -0.7), KT_{max} (r = -0.4).
- Az_{range} showed a positive correlation with ABz_{max} (r = 0.6), M_{agn} (r = 0.7),Ap_{max}, (r = 0.7), and SSN (r = 0.7), a negative correlation with Bz_{min} (r = -0.6), KT_{min} (r = -0.3), and Kp_{max} (r = -0.2).
- SSN displayed a positive correlation with ABz_{max} (r = 0.5), M_{agn} (r = 0.8), Ap_{max} (r = 0.6), and Az_{range} (r = 0.7), a negative correlation with Bz_{min} (r = -0.5), KT_{min} (r = -0.2), and Be_{max} (r = -0.5).

The correlation analysis highlights significant relationships between various FEID parameters, with notable strong negative and positive correlations indicating intertwined influences on Forbush events. For instance, the strong negative correlation between Bz_{min} and ABz_{max} suggests an inverse relationship, implying that when the minimal value of the Bz component decreases, the maximal absolute value tends to increase, and vice versa. Similarly, the positive correlations of $Bz_{min}$with Kp_{max} and A_{xym}suggest that increases in the minimal Bz component is associated with increases in geomagnetic activity and CR vector anisotropy. Comparing these results with more recent studies reveals some consistent findings as well as unique insights. Recent research has further investigated the correlations between solar activity, interplanetary parameters, and Forbush events, confirming many of our observed relationships.

SSN studies like those by [2,3] have shown strong correlations between sunspot numbers and geomagnetic indices, similar to our findings of SSN being positively correlated with Ap_{max}. These correlations underscore the influence of solar activity on cosmic ray modulation and geomagnetic disturbances. Our study's finding of a strong inverse relationship between Bz_{min} and AB_{zmax} aligns with the work of [12], who highlighted the importance of the Bz component in modulating cosmic rays and influencing geomagnetic storms the plasma beta parameters. The correlations involving plasma beta parameters (KT_{max} and KT_{min}) in our study are consistent with the research by [33], which discusses the impact of solar wind conditions, including plasma beta, on Forbush Decreases. Our findings that Kp_{max} and Ap_{max} are strongly correlated with other FEID parameters such as Bz_{min} and A_{xym} are supported by studies from recent years, such as those by [33], emphasizing the role of geomagnetic activity in characterizing

Forbush events. The correlation of anisotropy parameters ($A_{xym}$and Az_{range}) with Bz_{min}, KT_{min}, and M_{agn} is reflected in recent work by [34], who examined the anisotropic responses of cosmic rays to solar wind structures.

In Table 3, we calculated Pearson correlation coefficients for yearly mean values of 12 FEID parameters: Bz_{min} , ABz_{max} , KT_{max} , KT_{min} , Be_{max} , Be_{min} , M_{agn} , Kp_{max} , Ap_{max} , A_{xym} , Az_{range} , and SSN for Type 1 Forbush events from 1957 to 2019. The analysis of Pearson correlation coefficients of yearly mean FIED parameters for Type 1 Forbush events from 1957 to 2019 displayed in Table 2, shows significant relationships that are consistent with our findings in all events. Solar activity, interplanetary magnetic field components, and geomagnetic indices are all crucial in understanding the dynamics of Forbush events. These results reinforce the complex interplay between solar phenomena and their geomagnetic impacts, providing valuable insights for space weather research and prediction

- Bz_{min} showed a negative correlation with ABz_{max} (-0.9) and Ap_{max} (-0.6), while positively correlated with KT_{min} (0.6) and A_{xym} (0.6).
- ABz_{max} showed a strong negative correlation with Be_{min} (-0.9) and A_{xym} (-0.7), and a positive correlation with KT_{min} (-0.7).
- KT_{min} positively correlated with Bz_{min} (0.6), negatively correlated with ABz_{max} (-0.7), and highly correlated with A_{xym} (1.0).
- Be_{min} showed a strong negative correlation with KT_{min} (-1.0), Kp_{max} (-1.0), and A_{xym} (-1.0).
- M_{agn} positively correlated with Ap_{max} (0.5), Kp_{max} (0.5), and SSN (0.6).
- Kp_{max} showed a strong positive correlation with KT_{min} (1.0) and A_{xym} (1.0).
- A_{xym} showed it highly correlated with KT_{min} (1.0) positively and with Bz_{min} (0.6), and negatively correlated with Be_{Min} (-0.7).

Studies Our findings are consistent with [2,3], who found strong correlations between solar activity (e.g., SSN) and geomagnetic indices (e.g., Ap_{max} , Az_{range}).The strong negative correlation between Bz_{min} and ABz_{max} aligns with [12], indicating the significant role of the Bz component in geomagnetic storms.The correlation patterns involving Kp_{max} and Ap_{max} are supported by [29], who highlighted the importance of these indices in characterizing Forbush events. For the cosmic ray anisotropy, our results show correlations between anisotropy parameters (A_{xym} , Az_{range}) and Bz_{min} , KT_{min} , and M_{agn} which is in line with the work of [34].

In Table 4, we showed the Pearson correlation coefficients for yearly mean values of the 12 FEID parameters for Type 9 Forbush events from 1957 to 2019.

- Bz_{min} is strongly negatively correlated with ABz_{max} (-1.0) and positively correlated with KT_{min} (0.8) and A_{xym} (0.8).
- M_{agn} has a strong negative correlation with Bz_{min} (-1.0) and a positive correlation with KT_{min} (-0.9) and A_{xym} (-0.9).
- KT_{max} is negatively correlated with Bz_{min} (-0.4) and positively correlated with K_{Tmin} (-0.3).
- KT_{min} positively correlated with Bz_{min} (0.8), ABz_{max} (-0.9), and A_{xym} (1.0).
- Be_{min} is negatively correlated with KT_{min} (-0.6) and A_{xym} (-0.7).
- M_{agn} is positively correlated with Ap_{max} (0.6), SSN (0.7), and Az_{range} (0.6).
- K_{pmax} has strong positive correlations with KT_{min} (1.0) and A_{xym} (1.0).
- A_{xym} showed a high correlation with KT_{min} (1.0), Bz_{min} (0.8), and negatively correlated with ABz_{max} (-0.9).

The analysis of Pearson correlation coefficients of yearly mean FIED parameters for Type 9 Forbush events from 1957 to 2019 reveals several significant relationships among the parameters. Notably, the strong negative correlation between Bz_{min} and ABz_{max} and the positive correlations of Bz_{min} with KT_{min} and A_{xym} align with findings from recent studies, similar to findings by [2,3]. The negative correlation between Bz_{min} and ABz_{max} corroborates the findings of [12], which emphasize the influence of the Bz component in geomagnetic storms. The correlation patterns involving Kp_{max} and Ap_{max} are consistent with [29]. The significant correlations between anisotropy parameters (A_{xym} , Az_{range}) and Bz_{min}, K_{Tmin}, and M_{agn} align with the research by [34].

Overall, the results support the notion that solar activity, interplanetary magnetic field

components, and geomagnetic indices are crucial in understanding the dynamics of Forbush events. This analysis provides valuable insights into the statistical relationships between FIED parameters, reinforcing the complex interplay between solar phenomena and their geomagnetic impacts.

4. CONCLUSIONS

This study provides an extensive statistical analysis of the relationship between Forbush Effects and Interplanetary Disturbance (FIED) parameters from 1957 to 2019, using a comprehensive dataset of 7,482 events. The research primarily focuses on Type 1 and Type 9 Forbush events and examines key parameters such as AB_{zmax} , Kp_{max} , KT_{min}, KT_{max}, $Be_{max,}$ Be_{min} , M_{agn} , A_{xym} , Ap_{max} , Bz_{min} , AZ_{range} and SSN through descriptive statistics, distribution plots, time series analysis, and Pearson correlation coefficients.

Our correlation analysis indicated that the IMF components (Bz_{min} and ABz_{max}) correlates with each other as expected, correlates with the solar wind temperatures (KT_{max} and KT_{min}), though mildly, but not with the plasma density ($Be_{max,}$ and Be_{min}). IMF components also correlate with FD magnitude and geomagnetic indices and both the equatorial and the North-South components of the CR vector anisotropy and with SSN on the onset of FD. These trends were similar for all, Type 1 and Type 9 events though at different strengths.

The magnitude of FD for all events correlates strongly with the IMF components, Ap_{max} and SSN, mildly with solar wind temperatures and magnetic index Kp_{max}, while the FD magnitude of Type 1 events correlates mildly with most of the FEID parameters. The FD magnitude correlations with other FEID parameters for Type 9 events follow the trends of all events.

The SSN on the onset of FD, for all, Types 1 and 9 correlates with similar strength with FEID parameters, with only Be_{min} showing no correlation with SSN for all events, and Type 1 events but indicated mild negative correlation with SSN for Type 9 events.

The study shows how complex the relationships are between the sun's activity, the magnetic fields between planets, and geomagnetic indices. It also shows how strongly solar events affect cosmic ray modulation and geomagnetic disturbances. Consistent with recent studies, the findings highlight the importance of parameters like the Bz component in understanding and predicting space weather events. This research contributes valuable insights into the mechanisms driving Forbush Effects, enhancing our ability to forecast space weather and mitigate its impacts on technological systems and human activities.

DISCLAIMER (ARTIFICIAL INTELLIGENCE)

Author(s) hereby declare that NO generative AI technologies such as Large Language Models (ChatGPT, COPILOT, etc.) and text-to-image generators have been used during the writing or editing of manuscripts.

COMPETING INTERESTS

The authors have declared that no competing interests exist.

REFERENCES

1. Forbush SE. On the effects in cosmic-ray intensity observed during the recent magnetic storm. Physical Review, Physical Review. 1937;51(12):1108.
2. Richardson IG, Cane HV. Identification of interplanetary coronal mass ejections at 1 AU using multiple solar wind plasma composition anomalies Journal of Geophysical Research: Space Physics. 2004;109(A9):A09104.
3. Belov A, Eroshenko E, Yanke V, Oleneva, V, Abunin A, Abunina M, Papaioannou A, Mavromichalaki H. The global survey method applied to ground-level cosmic ray measurements. Solar Physics. 2018; 293(4):68.
4. Dorman LI. Cosmic Rays Variations and Space Exploration. North-Holland; 1974.
5. Lockwood JA. Forbush decreases in the cosmic radiation. Space Science Reviews. 1971;12(5):658.
6. Iucci N, Parisi M, Storini M, Villoresi G. High-speed solar-wind streams and galactic cosmic-ray modulation. Il Nuovo Cimento C. 1979;9(4):253.
7. Cane HV. Cosmic ray decreases and magnetic clouds Journal of Geophysical Research. 1993;98(A3):3509.
8. Cane HV. Coronal Mass Ejections and Forbush Decreases. Space Science Reviews. 2000;93(1-2):55.

9. Belov AV, Abunina MA, Abunin AA, Eroshenko EA, Oleneva VA, Yanke VG. Cosmic-ray vector anisotropy and local characteristics of the interplanetary medium. Geomagnetism and Aeronomy, 2017;57(4):389-397.
10. Belov A, Belov A, Abunin A, Abunina M, Eroshenko E, Oleneva V, Yanke V, Papaioannou A, Mavromichalaki H, Gopalswamy N, Yashiro S. Coronal mass ejections and non-recurrent forbush decreases. Solar Physics. 2014;289(10): 3949–3960.
11. Lingri D, Lingri, D, Mavromichalaki H, Belov A, Eroshenko E, Yanke, V., Abunin, A, Abunina M. Solar activity parameters and associated Forbush decreases during the minimum between Cycles 23 and 24 and the ascending phase of Cycle 24. Solar Physics. 2016;291(3):1025-1041
12. Gopalswamy N, Yashiro S, Akiyama S, Mäkelä P, Michalek G. Properties and geoeffectiveness of magnetic clouds during solar cycles 23 and 24 Journal of Geophysical Research: Space Physics. 2015;120(11):9221.
13. Belov A, Guschina, RT., & Sirotina, I. V. The modulation spectrum of cosmic ray variations during Cycles 19-22 of the Sun. In D. A. Leahy, R. B. Hicks, & D. Venkatesan (Eds.), Proceedings of the 23rd International Cosmic Ray Conference. 1993;3:605. World Scientific.
14. Belov A, Eroshenko E, Oleneva V, Struminsky A, Yanke V. What determines the magnitude of Forbush decreases? Advances in Space Research. 2001; 27(3):625.
15. Belov A, Eroshenko E, Yanke V, Mavromichalaki H, Plainaki C. A study of the ground level enhancement of 23 February 1956. Advances in Space Research. 2005;35(4):699.
16. Belov A, Abunin A, Abunina M, Eroshenko E, Oleneva V, Yanke V, Papaioannou A, Mavromichalaki H. Galactic cosmic ray density variations in magnetic clouds. Solar Physics. 2015;290:1429–1444.
17. Lingri D, Mavromichalaki H, Belov A, Eroshenko E, Yanke V, Abunin A, Abunina M. Solar activity parameters and associated Forbush decreases during the minimum between Cycles 23 and 24 and the ascending phase of Cycle 24.Solar Physics. 2016;291(I. 3):1429–1444.
18. Chertok IM, Abunina MA, Abunin AA, Belov AV, Grechnev VV. Relationship between the magnetic flux of solar eruptions and the Ap index of geomagnetic storms Solar Physics. 2015;290(I. 2):627–633.
19. Belov A, Abunin A, Abunina M, Eroshenko E, Oleneva V, Yanke V, Papaioannou A, Mavromichalaki H. Galactic cosmic ray density variations in magnetic clouds Solar Physics. 2015;290(I. 5):1429–1444.
20. Belov AV, Abunin AA, Abunina MA, Eroshenko EA., Oleneva VA., Yanke VG. Density variations of galactic cosmic rays in magnetic clouds Geomagnetism and Aeronomy. 2015;55(4):430-441.
21. Kryakunova O, Belov A, Abunin A, Abunina M, Eroshenko E, Malimbayev A, Tsepakina I, Yanke V. Recurrent and sporadic Forbush-effects in deep solar minimum Journal of Physics – Conference Series. 2015;632.
22. Belov A, Abunin A, Abunina M, Eroshenko E, Oleneva V, Yanke V, Papaioannou A, Mavromichalaki H, Gopalswamy N, Yashiro S. Coronal mass ejections and non-recurrent Forbush decreases. Solar Physics. 2014;289(I.10):3949–3960.
23. Abunina M, Abunin A, Belov A, Gaidash S, Yanke V, Tassev Y, Velinov P, Mateev L, Tonev P. Properties of magnetic fields in coronal holes and geo-effective disturbances in solar cycle 24 Comptes rendus de l'Acad´emie Bulgare des Sciences. 2014;67(N. 5):699–704.
24. Chertok IM, Grechnev VV, Belov AV, Abunin AA. The magnetic flux of EUV arcade and dimming regions as a relevant parameter for early diagnostics of solar eruptions - sources of non-recurrent geomagnetic storms and Forbush decreases Solar Physics. 2013;283(I. 2):557–563.
25. Chertok IM, Abunin AA, Belov AV, Grechnev VV. Dependence of Forbush-decrease characteristics on parameters of solar eruptions Journal of Physics – Conference Series. 2013;409(I. 1).
26. Abunina M, Papaioannou A, Gerontidou M, Paschalis P, Abunin A, Gaidash S, Tsepakina I, Malimbayev A, Belov A, Mavromichalaki H, Kryakunova O, Velinov P. Forecasting geomagnetic conditions in near-Earth space Journal of Physics – Conference Series. 2013;409(I. 1).
27. Papailiou M, Mavromichalaki H, Abunina M., Belov A, Eroshenko E, Yanke V, Kryakunova O. Forbush decreases associated with western solar sources and

geomagnetic storms: a study on precursors Solar Physics. 2013;283(I. 2):557–563.
28. Belov AV, Obridko VN, Shelting BD. Correlation between the near-earth solar wind parameters and the source surface magnetic field Geomagnetism and Aeronomy. 2006;46(I. 4):430–437.
29. Abunin AA, Abunina MA, Belov AV, Eroshenko EA, Oleneva VA, Yanke VG. Forbush effects with a sudden and gradual onset. Geomagnetism and Aeronomy. 2012;52(3):292-299
30. Belov AV, Eroshenko EA, Yanke VG, Oleneva VA, Abunina MA, Abunin AA. Global survey method for the world network of neutron monitors. Geomagnetism and Aeronomy. 2018; 58(3):356-372. 31.
31. Available:https://www.sidc.be/silso/exthemi num
32. Fisher RA. Frequency Distribution of the Values of the Correlation Coefficient in Samples from an Indefinitely Large Population Biometrika. 1915;10(4):507.
33. Echer E, Gonzalez WD, Tsurutani BT. Statistical Studies of Geomagnetic Storms with Peak Dst≤−50nT from 1957 to 2008. Journal of Atmospheric and Solar-Terrestrial Physics, Influence of Solar Activity on Interplanetary and Geophysical Phenomena. 2011;73(11): 1454-1459.
34. Oh S, Kim T, Yi Y, Statistical reality of globally non-simultaneous Forbush decrease events. journal of Geophysical Research. 2009;114:a11102, DOI:10.1029/2009JA014190,.

Peer-review history:
The peer review history for this paper can be accessed here:
https://prh.globalpresshub.com/review-history/1653